NANO LETTERS

pubs.acs.org/NanoLett Letter

Colossal Magnetoelectric Effect in Core−Shell Magnetoelectric Nanoparticles

Ping Wang, Elric Zhang, Dennis Toledo, Isadora Takako Smith, Brayan Navarrete, Nathaniel Furman, Alexandro Franco Hernandez, Mackenson Telusma, Dwayne McDaniel, Ping Liang, and Sakhrat Khizroev*

Cite This: https://dx.doi.org/10.1021/acs.nanolett.0c01588 Read Online

ACCESS | Metrics & More | Article Recommendations | Supporting Information

ABSTRACT: Magnetoelectric coefficient values of above 5 and 2 V cm^{-1} Oe^{-1} in 20 nm $CoFe_2O_4$−$BaTiO_3$ and $NiFe_2O_4$−$BaTiO_3$ core−shell magnetoelectric nanoparticles were demonstrated. These colossal values, compared to 0.1 V cm^{-1} Oe^{-1} commonly reported for the 0−3 system, are attributed to (i) the heterostructural lattice-matched interface between the magnetostrictive core and the piezoelectric shell, confirmed through transmission electron microscopy, and (ii) in situ scanning tunneling microscopy nanoprobe-based ME characterization. The nanoprobe technique allows measurements of the ME effect at a single-nanoparticle level which avoids the charge leakage problem of traditional powder form measurements. The difference in the frequency dependence of the ME value between the two material systems is owed to the Ni-ferrite cores becoming superparamagnetic in the near-dc frequency range. The availability of novel nanostructures with colossal ME values promises to unlock many new applications ranging from energy-efficient information processing to nanomedicine and brain−machine interfaces.

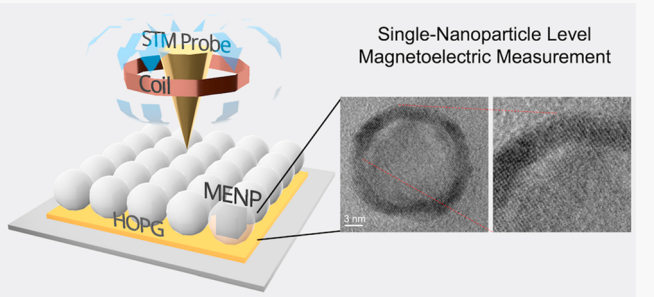

KEYWORDS: *Colossal Magnetoelectric Effect, $CoFe_2O_4$−$BaTiO_3$, $NiFe_2O_4$−$BaTiO_3$, Core−Shell Magnetoelectric Nanostructures, Brain−Machine Interface, Artificial Intelligence*

Over the past decade, there has been a growing interest in magnetoelectric nanoparticles (MENPs).[1] Many new applications of MENPs have emerged, ranging from spintronics for energy-efficient information processing to nanomedicine for enabling personalized precision medicine.[2−8] Arguably, the wireless brain−machine interface (BMI) would be one of the most impactful of these applications; it is hard to overestimate the significance of the availability of such technology for medicine, particularly related to treatment of neurodegenerative diseases and brain tumors, as well as for improving our fundamental understanding of the brain and interfacing the human brain with artificial intelligence (AI).[9] Owing to the presence of the magnetoelectric (ME) effect, unlike any other nanoparticles, MENPs offer a way to use a voltage to control the electron spin in spintronic devices and, reciprocally, to use remotely controlled magnetic fields to access local intrinsic electric fields that in turn underlie fundamental physiological conditions at the molecular level. The MENPs' most essential property is their relatively high ME coefficient, which reflects intrinsic coupling between magnetic and electric fields. Hence, realization of the aforementioned, groundbreaking MENPs' applications strongly depends on the availability of nanoparticles with an adequately high ME coefficient.

There are two basic types of magnetoelectric materials: (i) single-phase structures such as multiferroics in which magnetic and electric fields are intrinsically coupled, for example, through the spin−orbit interaction (L−S coupling) in one single phase and (ii) multiphase heterostructured composites in which spatially separated magnetostrictive and piezoelectric components are connected through an interface. Due to the contradiction between the traditional mechanism of ferroelectric order, namely, unoccupied d-orbitals, and the magnetic moment generated by partially filled d-orbitals in ferrites, single-phase multiferroic materials have been rarely reported.[10−13] As for multiphase heterostructured ME composites, magnetoelectricity originates at the interface between these two components.[14−16] To date, the highest values, on the order of 10 V cm^{-1} Oe^{-1}, have been reported mostly for relatively large size heterostructured composites such as 2−2

Received: April 12, 2020
Revised: July 7, 2020
Published: July 8, 2020

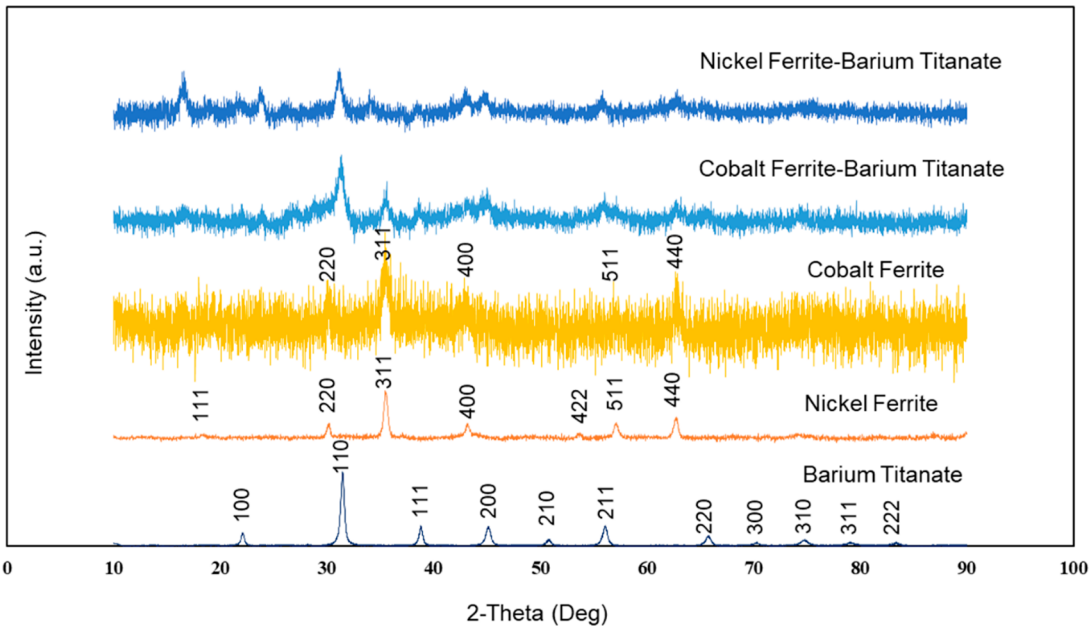

Figure 1. X-ray diffraction (XRD) measurements showing peak shifts of Co- and Ni-ferrite cores and the barium titanate shell during the formation of $CoFe_2O_4$−$BaTiO_3$ and $NiFe_2O_4$−$BaTiO_3$ core−shells. To improve the clarity of the figure, the top three scans are multiplied by an intensity factor of 3.

laminated composites,[17−25] not for 0−3 particulate composites such as MENPs. Commonly reported experimental values for 0−3 particulate ME composites are on the order of 0.1 V cm^{-1} Oe^{-1} (=100 mV cm^{-1} Oe^{-1}).[26−28] Hereinafter, we would like to note that the paper follows the ME coefficient units of V cm^{-1} Oe^{-1} instead of the traditional mV cm^{-1} Oe^{-1}. The most studied composition is $CoFe_2O_4$−$BaTiO_3$ made of the magnetostrictive spinel core, $CoFe_2O_4$, and the piezoelectric perovskite shell, $BaTiO_3$.[29] The physical properties of these materials can be adjusted by a compositional substitution of transition metals, e.g., using nickel instead of cobalt. The size of these nanostructures can be controlled in a range from below 20 nm to over 55 nm by varying the core size ranging from 3 to 15 nm. Thermal decomposition and seed-mediated growth methods have been employed to synthesize Co- and Ni-ferrite cores.

The physics of multiferroics is usually described by Landau−Ginsburg−Devonshire phenomenological thermodynamic theory.[30−32] According to this theory, the cross-field term of the second order expansion of the free energy of a multiferroic material, W, is given by eq 1

$$W = -\alpha_{ij} H_i E_j \tag{1}$$

where E and H stand for electric and magnetic fields, respectively, and α is the magnetoelectric coefficient tensor. Owing to this energy cross-field term, application of a magnetic field would lead to a change of the electric polarization, while application of an electric field would lead to a change of the magnetization. These two relations, known as direct and converse magnetoelectric effects, respectively, can be expressed through eqs 2 and 3

$$P_i = \alpha_{ij} H_j \tag{2}$$

$$M_i = \alpha_{ij} E_j \tag{3}$$

Despite the rapidly emerging interest in the aforementioned MENP-enabled applications, to date, the ME effect in MENPs has only been investigated in powder form.[33−35] It is noteworthy that the powder form does not accurately provide the ME effect of an individual nanoparticle due to various challenges.[36] For example, according to the most popular ME measurement technique, a powder of MENPs is exposed to a mechanical pressure so that nanoparticles are in physical contact with each other;[37−40] then, the net collective ME effect is measured as a voltage change in response to a magnetic field or, reciprocally, as a magnetic moment change in response to an electric field. For the latter, the effect is also known as the converse ME effect. The net effect in the powder measurements depends also on the pressure between adjacent nanoparticles as well as the morphology, volume fraction, and orientation distribution of particles of both phases.[15,20,41] Ideally, for a basic 0−3 particulate composite, the magnetostrictive phase, with the lower resistance, should be evenly distributed in the piezoelectric matrix to maintain adequate insulation of the composite. However, in practical powder measurement systems, some charge leakage paths can be formed through the magnetostrictive phase, making it difficult to fully polarize the piezoelectric phase. Consequently, the volume fraction of the magnetostrictive phase in the piezoelectric matrix is limited by this charge leakage problem.[42] Therefore, it is not surprising that the ME values reported from different laboratories vary in a relatively wide range, typically from below 0.001 V cm^{-1} Oe^{-1} to over 0.1 V cm^{-1} Oe^{-1}.[43] To minimize the leakage problem, 2−2 type laminated heterostructured ME composites were developed where magnetostrictive layers are separated by piezoelectric layers to prevent the leakage problem. Indeed, several articles have reported ME values above 1 V cm^{-1} Oe^{-1} for heterostructures with 2−2 type connectivity. Such values are significantly higher than those for heterostructures with 0−3/1−3 connectivity of the same composition.[17,18,20,44−46] It is noteworthy that, to the best of our knowledge, no studies of the ME effect in MENPs have been reported at a single-nanoparticle level. ME

https://dx.doi.org/10.1021/acs.nanolett.0c01588
Nano Lett. XXXX, XXX, XXX−XXX

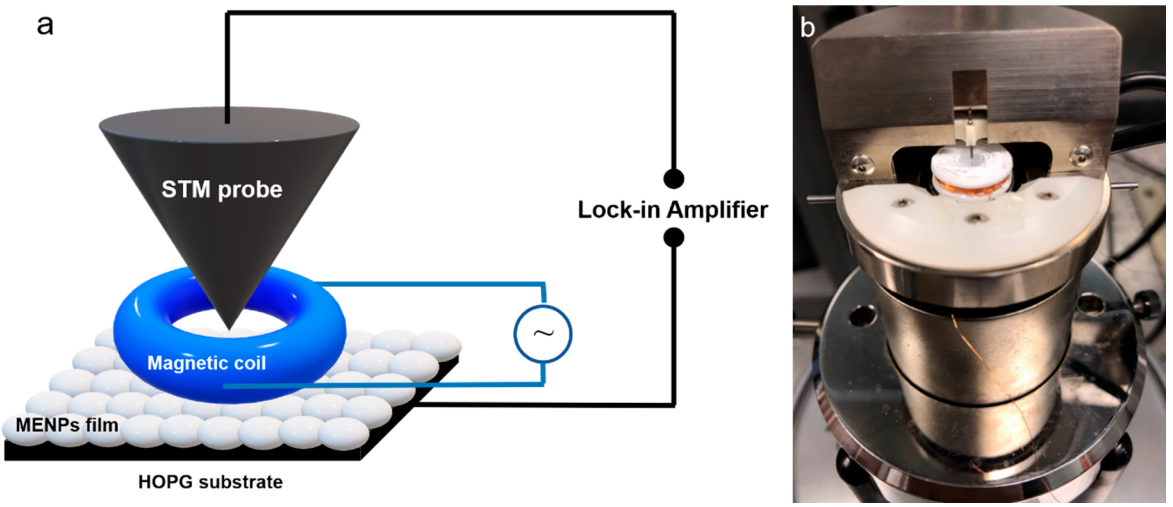

Figure 2. (a) Diagram of the STM-based nanoprobe setup for single-nanoparticle level ME measurements. (b) Photograph of the setup.

measurements at nanoscale level could completely eliminate the destructive charge leakage effect.

Therefore, in this study, a ME measurement technique, based on a scanning tunneling microscope (STM) probe, has been implemented with the purpose to overcome the leakage problem of the traditional approach and to create MENPs with ME values as high as those reported for 2−2 type laminated heterostructured ME composites. An STM nanoprobe has been employed as one electrode instead of utilizing a large size conductive plate/film as in the traditional setup. This technique is not only immune to the interparticle forces but also could eliminate the charge leakage problem. According to basic "back-of-the-envelope" physics calculations, given a lattice-matched interface, assuming the magnetostriction constant of the core and the piezoelectric constant of the shell are equal to the values for their bulk counterparts, i.e., −200 ppm and ∼190 pC/N, respectively, the ME coefficient, α, could be above 10 V cm^{-1} Oe^{-1}.[47,48] Further, given that the elastic coefficients are expected to significantly increase as characteristic sizes of these structures are reduced into the nanoscale, significantly higher values of α should be expected. Indeed, an increase of the magnetostriction by 2 orders of magnitude, compared to the bulk values, has been reported.[49] Therefore, there must be plenty of room to achieve a substantially larger ME coefficient at the nanoscale, compared to the value on the order of 0.1 V cm^{-1} Oe^{-1} for 0−3 particulate composites that has been reported to date. Considering the difficulty of unambiguously measuring the ME coefficient, it is not straightforward to optimize the synthesis method. Undoubtedly, there is an opportunity for research concerning the synthesis of inorganic−inorganic, lattice-matched core−shell MENPs. Therefore, this study aims to significantly increase the ME coefficient by conducting single-nanoparticle level ME measurements, as a feedback for synthesis optimization, to achieve a lattice-matched core−shell configuration which can be confirmed through TEM.

Core−shell MENPs of two different compositions, $CoFe_2O_4$−$BaTiO_3$ and $NiFe_2O_4$−$BaTiO_3$, both with a diameter of approximately 20 nm, were synthesized according to a thermal decomposition method for core synthesis, oil phase transferred to hydrophilic phase of cores, and sol−gel method for MENP synthesis, as described in detail (section S1 in the Supporting Information). X-ray diffraction (XRD) analysis of these nanostructures is summarized in Figure 1. The corresponding normalized peaks demonstrate the purity of cobalt ferrite, nickel ferrite, and barium titanate as well as the shift of each corresponding peak in core−shell configurations compared to those in isolated compositions.[50] As a representative example, the main characteristic peak (110) of barium titanate shifts left in the core−shell configuration of $CoFe_2O_4$−$BaTiO_3$, as illustrated in a zoomed-in version in Figure S10. The positions and relative peaks match well with cobalt ferrite PDF card 01-083-4766, nickel ferrite PDF card 00-054-0964, and barium titanate PDF card 04-012-8129, respectively. The ME coefficient, α, was measured according to the following contact nanoprobe method, as illustrated in Figure 2. First, a thin layer of synthesized MENPs was deposited on a highly oriented pyrolytic graphite (HOPG) substrate. Then, a nanoscale contact was established between the layer and a STM nanoprobe made of platinum/iridium (see Figure S7 for the SEM image of a STM probe). The nanoprobe was attached to the Z-nanopositioner of a Bruker scanning probe microscope (SPM) Multimode. A permanent magnet assembled inside the scanner provides a dc bias magnetic field above 1000 Oe. A multiturn coil was placed around the contact to generate a perpendicular ac magnetic field. An electric current up to 60 mA through the coil resulted in a field up to 100 Oe. Simulations of various magnetic field strengths produced by the multiturn coil at ac voltages ranging from 0.1 to 1 V were conducted through COMSOL software, as shown in Figure S8. In turn, owing to the ME effect of the nanoparticles in the layer, application of a magnetic field induced a voltage change between the HOPG substrate and the nanoprobe, $V = Pd$, where P is the induced polarization and d is the thickness of the layer. The resulting ME coefficient was found according to eq 2. Note that the lateral resistivity of the nanoparticle layer on the HOPG was unreadable using a multimeter. For each sample, seven identical measurements were conducted on different spots on the nanoparticle layer. The averaged ME coefficient was calculated based on multiple measurements. In most cases, more than one nanoparticle contributes to the measured ME coefficients in order to acquire a more stable ME voltage. This single-nanoparticle-level ME measurement was used as feedback to optimize the key parameters of the described synthesis approach. Typical TEM images of thus fabricated 20 nm $CoFe_2O_4$−$BaTiO_3$ and

https://dx.doi.org/10.1021/acs.nanolett.0c01588
Nano Lett. XXXX, XXX, XXX−XXX

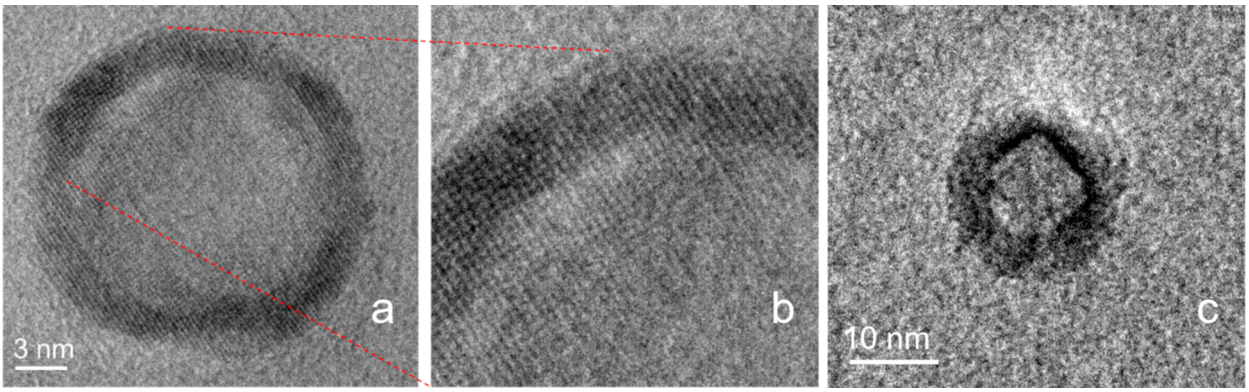

Figure 3. (a) TEM image of a 20 nm $CoFe_2O_4$–$BaTiO_3$ MENP. (b) A zoomed-in version shows the lattice-matched interface between the core and the shell. (c) TEM image of a 20 nm $NiFe_2O_4$–$BaTiO_3$ MENP.

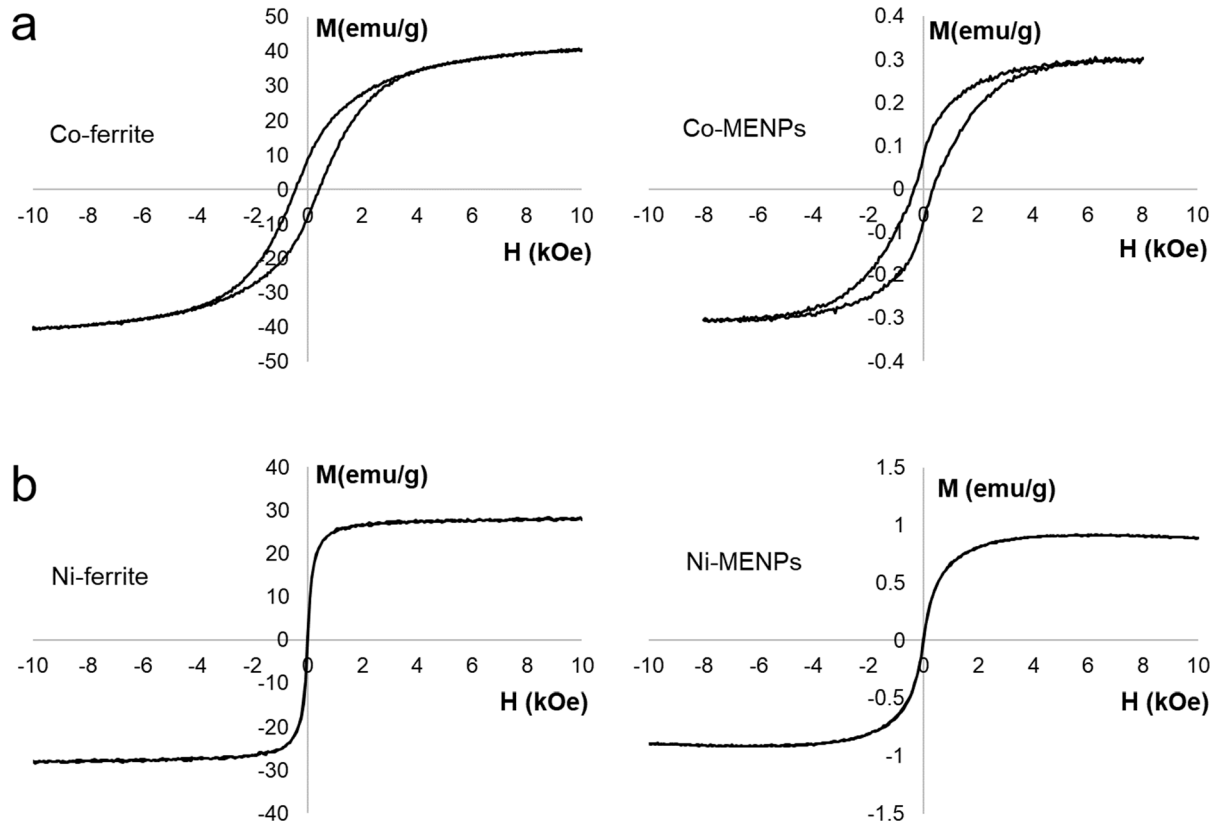

Figure 4. dc M–H loops measured via AGM of (a) 15 nm Co-ferrite nanoparticles and Co-ferrite-based 20 nm MENPs and (b) 10 nm Ni-ferrite nanoparticles and Ni-ferrite-based 20 nm MENPs.

$NiFe_2O_4$–$BaTiO_3$ MENPs are shown in Figure 3a and c, respectively. A zoomed-in version of the first system in Figure 3b clearly shows the lattice matching between the crystal lattices of the core and the shell.

Again, the main goal of this Letter is to present the key results, particularly the colossal ME values of the lattice-matched core–shell MENPs. The key results are illustrated in 20 nm MENPs. It is noteworthy that the same approach can be used to synthesize the two MENP systems in a wide size range, as summarized in Figures S5 and S6, respectively. To control the size of thus synthesized MENPs, we varied the size of the core of the core–shell structures. Parts a–c of Figure S5 show the Co-ferrite nanoparticles with diameters of 7, 11, and 15 nm, respectively, and parts d–f of Figure S5 show the respective Co-ferrite-based MENPs of the three average sizes, 15, 18, and 20 nm, respectively. Similarly, parts a–c of Figure S6 show the Ni-ferrite nanoparticles with diameters of 3, 10, and 15 nm, respectively, and parts d–f of Figure S6 show the respective Ni-ferrite-based MENPs of the three average sizes, 12, 20, and 50 nm, respectively. In addition, to further control the sizes of the synthesized MENPs, atomic force microscopy (AFM) imaging was conducted. Although AFM is prone to drift and other errors, the measurements supported the basic synthesis strategy. As an example, AFM studies of two different sizes of MENPs are summarized in Figure S9.

Magnetization versus magnetic field dependencies, i.e., M–H loops, for these two MENP systems are shown in Figure 4. The measurements were taken at room temperature with alternating gradient magnetometry (AGM) with a sensitivity of 10^{-6} emu. Also shown are the M–H loops for the magnetic

https://dx.doi.org/10.1021/acs.nanolett.0c01588
Nano Lett. XXXX, XXX, XXX–XXX

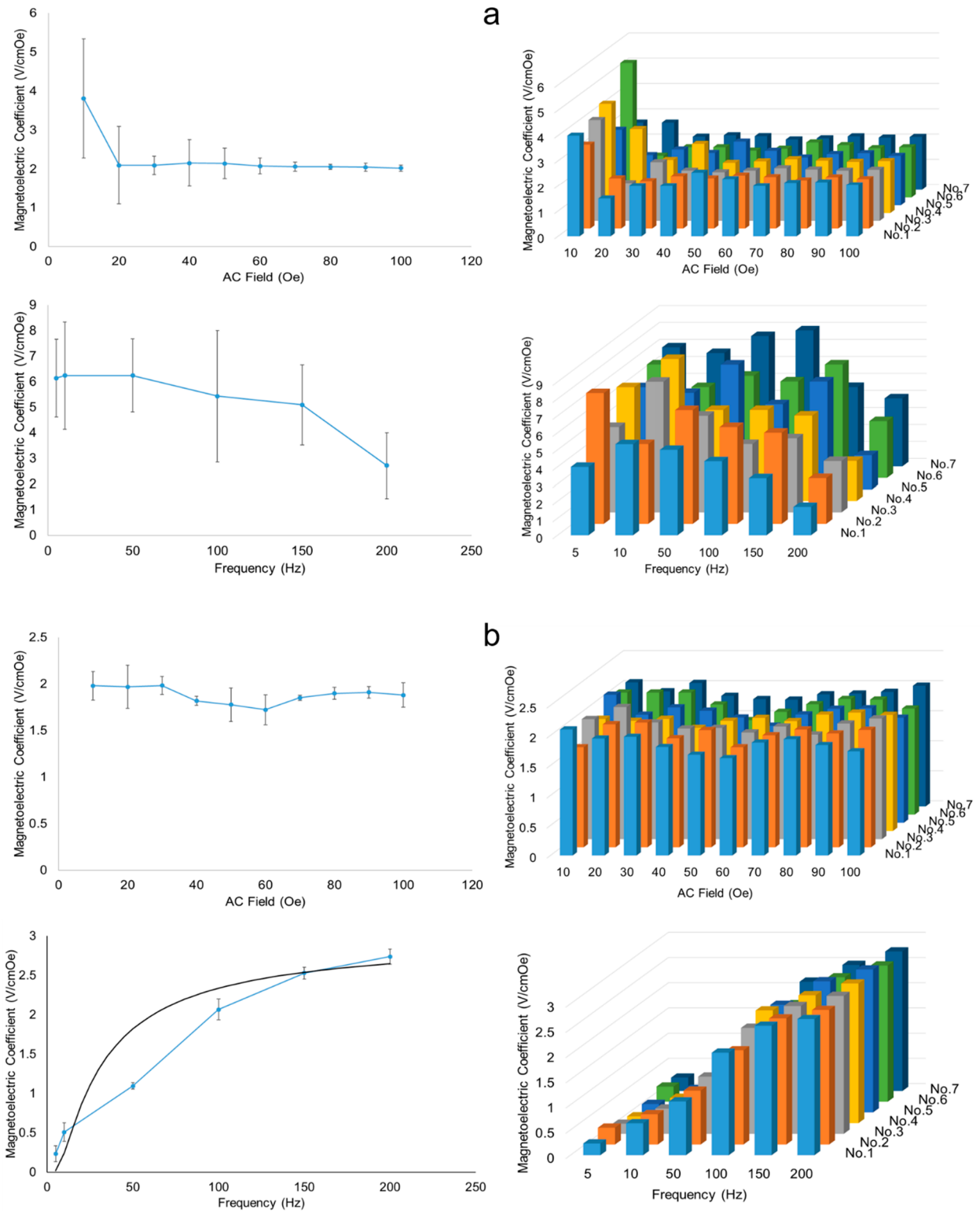

Figure 5. Nanoprobe-based ME coefficient measurements: (a) Co-ferrite MENPs: the ME coefficient is shown as a function of the ac field strength (at 100 Hz) (top row) and frequency (at 9 Oe) (bottom row). Each dependence is shown as a 3D chart and a 2D plot with an error bar. The error bar for each point is obtained as a result of averaging over seven measurements. (b) Ni-ferrite MENPs: the ME coefficient is shown as a function of the ac field strength (at 100 Hz) (top row) and frequency (at 9 Oe) (bottom row). The solid black line in the ME frequency dependence figure also shows a theoretical curve assuming a stability ratio of 20.

core nanoparticles, $CoFe_2O_4$ and $NiFe_2O_4$, of which the two MENP systems were made. As expected, the saturation magnetization of MENPs is significantly lower than that of their respective magnetic cores. It can be noted that these measurements were conducted in a powder form. Therefore, it is not possible to directly quantify the magnetic anisotropy of these nanostructures. To be able to directly quantify the magnetic anisotropy values, it is important to identify "easy"

https://dx.doi.org/10.1021/acs.nanolett.0c01588
Nano Lett. XXXX, XXX, XXX−XXX

magnetic orientations and conduct measurements in both directions, parallel and perpendicular, to these preferred orientations. In contrast, in the powder form, all of the orientations are equivalently mixed up and therefore there are no preferred orientations. However, indirectly, comparative conclusions about the magnetic anisotropy of these systems could be made. Indeed, it could be seen that the Co-ferrite magnetic cores do not reach their saturation magnetization even at the highest applied magnetic field of 10 kOe. In comparison, the Ni-ferrite magnetic cores reach their saturation magnetization at about 1 kOe. Furthermore, as expected for this core size range, the Ni-ferrite cores and the MENPs made of these cores are in the superparamagnetic state; i.e., their $M-H$ loops show no hysteresis. In contrast, the Co-ferrite cores and the MENPs made of these cores show visible hysteresis loops, with coercivity fields of 480 and 320 Oe, respectively. As described below in more detail, the difference between the two systems is due to the significant difference, by approximately an order of magnitude, between their magnetocrystalline anisotropy energies and the resulting difference in the stability ratio.[51,52]

The single-nanoparticle level, nanoprobe-based ME measurements for the two studied systems, Co- and Ni-ferrite-based 20 nm MENPs, as a function of the field strength and frequency, are summarized in Figure 5a and b, respectively. The Co- and Ni-ferrite MENPs have shown ME coefficients in the near-dc frequency range on the order of 6 V cm^{-1} Oe^{-1} and less than 0.1 V cm^{-1} Oe^{-1}, respectively. However, the frequency dependences of the MENPs of these two materials are dramatically different. The ME coefficient of the Co-ferrite-based MENPs shows a frequency roll-off dependence, particularly after 100 Hz, as explained below in more detail. In contrast, the ME coefficient for the Ni-ferrite-based MENPs strongly depends on the frequency; the coefficient significantly increases to over 2 V cm^{-1} Oe^{-1} for the highest frequency value of 200 Hz. The frequency dependence can be explained by the transition between the ferromagnetic and superparamagnetic states of the MENPs' magnetic cores. The stability ratio for the magnetic core is defined as

$$S = KV/k_BT \quad (4)$$

where K is the magnetic anisotropy energy density, V is the volume of the core component, k_B is the Boltzmann constant, and T is the ambient temperature. For a shelf life (nonvolatility duration) of 10 years, the stability ratio should be larger than approximately 40.[53] Because of the exponential dependence of the collective spin relaxation process, reduction of the stability ratio only by a factor of 2, i.e., down to 20, would reduce the shelf life down to the order of 1 s. For example, for the 15 nm Co-ferrite nanoparticles, with a magnetocrystalline anisotropy, K, of 10^6 J/m^3, and neglecting shape anisotropy, the stability ratio, S, would be on the order of $10^6 \times (4/3)\pi(7.5 \times 10^{-9})^3/(4 \times 10^{-21}) \sim 200$. For comparison, for the 10 nm Ni-ferrite nanoparticles, with a magnetocrystalline anisotropy, K, of 10^5 J/m^3, i.e., approximately an order of magnitude smaller, the stability ratio, S, would be on the order of $10^5 \times (4/3)\pi(5 \times 10^{-9})^3/(4 \times 10^{-21}) \sim 20$. Therefore, the shelf life for the Co- and Ni-ferrite nanoparticles would be greater than 10 years and on the order of 1 s, respectively. It should be noted that this analysis is a relatively rough evaluation of the stability ratios for the two nanostructures. The precise values of the magnetic anisotropy depend also on the shape anisotropy (in practice, in the size range under study, these nanoparticles are not perfect spheres, as can be noted from the shown TEM images) as well as the surface contribution to the net effect (the smaller the size, the larger the surface to volume contribution). To some approximations, this difference in the stability ratio between the two nanostructures could explain the observed frequency dependences. In the case of dc AGM measurements, the Ni-ferrite-based MENPs are superparamagnetic and thus display a weak magnetoelectric effect. However, as soon as the frequency is increased above approximately 1 Hz, which implies a measurement time of less than 1 s, the nanoparticles are not superparamagnetic during the measurement time. This explains the exponentially fast rise of the ME value corresponding to an increase in frequency. A theoretical curve, assuming a stability ratio of 20, is also plotted as a solid black line in the left bottom corner in Figure 5b. The relatively smaller frequency roll-off dependence of the Co-ferrite-based MENPs, especially for the points after 100 Hz, could be explained by the contribution of the inductance into the impedance of the electromagnet used to measure the ME coefficient. Indeed, the inductive impedance, R_L, of the electromagnetic system increases with frequency as $R_L \sim 2\pi fL$, where L is the inductance and f is the frequency. For example, at a frequency of 100 Hz and an inductance of 1 mH (measured with a standard inductance meter), the reactive impedance (due to the inductance) is $R_L \sim 1\ \Omega$. Given the real resistance of the coil on the order of 5 Ω, the increased contribution of the inductive component to the net impedance can explain the rolling-off frequency dependence after approximately 100 Hz. In the case of the Ni-ferrite-based MENPs, we do not "see" this coil effect dependence of the frequency roll-off because it is overshadowed by the more significant effect due to the aforementioned superparamagnetic-to-non-superparamagnetic transition.

This study has directly demonstrated, through TEM imaging, the creation of crystal lattice matching between the two main components of the inorganic−inorganic crystalline core−shell nanoparticles under study. The two specific types of 20 nm MENPs, Co- and Ni-ferrite-based MENPs, differed in their core compositions and their core sizes, 15 and 10 nm, respectively, while having the same shell composition of barium titanate. These nanostructures have been obtained as a result of the discussed synthesis method using the nanoprobe ME measurement as an optimization feedback. The perfect interface coupling and the optimized volume fraction of the magnetostrictive core being selected as 0.5 could explain the colossal ME coefficient of above 5 and 2 V cm^{-1} Oe^{-1} for Co- and Ni-ferrite-based 20 nm MENPs, respectively.[54,55] It is more than an order of magnitude improvement compared to previous measurements reported elsewhere.[56] It is noteworthy that these values are significantly closer to the values obtained based on the above theoretical analysis and other theoretical studies elsewhere.[17] The ME coefficients in both Co- and Ni-based MENPs were independent of the applied ac magnetic field strength and found to be in reasonable agreement with other theoretical papers.[57] These colossal ME values have a great potential to unlock the aforementioned novel applications in energy-efficient information processing and nanomedicine.

https://dx.doi.org/10.1021/acs.nanolett.0c01588
Nano Lett. XXXX, XXX, XXX−XXX

■ ASSOCIATED CONTENT

Supporting Information

The Supporting Information is available free of charge at https://pubs.acs.org/doi/10.1021/acs.nanolett.0c01588.

Descriptions of the nanoparticle fabrication processes (both for the MENPs and their magnetostrictive seeds) as well as descriptions of the characterization methods (PDF)

■ AUTHOR INFORMATION

Corresponding Author

Sakhrat Khizroev − *Department of Electrical and Computer Engineering, University of Miami, Coral Gables, Florida 33146, United States*; Email: skhizroev@miami.edu

Authors

Ping Wang − *Department of Electrical and Computer Engineering, University of Miami, Coral Gables, Florida 33146, United States; Department of Electrical and Computer Engineering, Florida International University, Miami, Florida 33174, United States*; orcid.org/0000-0001-7426-3151

Elric Zhang − *Department of Electrical and Computer Engineering, University of Miami, Coral Gables, Florida 33146, United States*

Dennis Toledo − *Department of Electrical and Computer Engineering, University of Miami, Coral Gables, Florida 33146, United States; Department of Electrical and Computer Engineering, Florida International University, Miami, Florida 33174, United States*; orcid.org/0000-0002-2700-1180

Isadora Takako Smith − *Department of Electrical and Computer Engineering, University of Miami, Coral Gables, Florida 33146, United States*

Brayan Navarrete − *Department of Electrical and Computer Engineering, University of Miami, Coral Gables, Florida 33146, United States*

Nathaniel Furman − *Department of Electrical and Computer Engineering, University of Miami, Coral Gables, Florida 33146, United States*

Alexandro Franco Hernandez − *Department of Mechanical and Materials Engineering, Florida International University, Miami, Florida 33174, United States*

Mackenson Telusma − *Department of Mechanical and Materials Engineering, Florida International University, Miami, Florida 33174, United States*

Dwayne McDaniel − *Department of Mechanical and Materials Engineering, Florida International University, Miami, Florida 33174, United States*

Ping Liang − *Cellular Nanomed, Irvine, California 92697, United States*

Complete contact information is available at: https://pubs.acs.org/10.1021/acs.nanolett.0c01588

Notes

The authors declare no competing financial interest.

■ ACKNOWLEDGMENTS

This material is based upon work supported by the Defense Advanced Research Projects Agency (DARPA) and Naval Information Warfare Center, Pacific (NIWC Pacific) under Contract No. N66001-19-C-4019. Any opinions, findings, and conclusions or N6600119C4019 recommendations expressed in this material are those of the author(s) and do not necessarily reflect the views of the DARPA or NIWC Pacific. In addition, this work has been partially supported by National Science Foundation (NSF) under Award Nos. ECCS-1810270 and ECCS-0939514, Air Force Office of Scientific Research (AFOSR) under Award No. FA9550-18-1-0527, and Office of Naval Research (ONR) under Award No. 11594311.

■ REFERENCES

(1) Khizroev, S.; Liang, P. Engineering future medicines with magnetoelectric nanoparticles: wirelessly controlled, targeted therapies. *IEEE Nanotechnology Magazine* **2020**, *14* (1), 23−29.

(2) Ramesh, R.; Spaldin, N. A. Multiferroics: progress and prospects in thin films. *Nat. Mater.* **2007**, *6* (1), 21−29.

(3) Spaldin, N. A.; Fiebig, M. The renaissance of magnetoelectric multiferroics. *Science* **2005**, *309* (5733), 391−392.

(4) Hur, N.; Park, S.; Sharma, P. A.; Ahn, J. S.; Guha, S.; Cheong, S. W. Electric polarization reversal and memory in a multiferroic material induced by magnetic fields. *Nature* **2004**, *429* (6990), 392−395.

(5) Scott, J. F. Data storage - Multiferroic memories. *Nat. Mater.* **2007**, *6* (4), 256−257.

(6) Fiebig, M. Revival of the magnetoelectric effect. *J. Phys. D: Appl. Phys.* **2005**, *38* (8), R123−R152.

(7) Rodzinski, A.; Guduru, R.; Liang, P.; Hadjikhani, A.; Stewart, T.; Stimphil, E.; Runowicz, C.; Cote, E.; Altman, N.; Datar, R.; Khizroev, S. Targeted and controlled anticancer drug delivery and release with magnetoelectric nanoparticles. *Sci. Rep.* **2016**, *6*, 20867.

(8) Nair, M.; Guduru, R.; Liang, P.; Hong, J. M.; Sagar, V.; Khizroev, S. Externally controlled on-demand release of anti-HIV drug using magneto-electric nanoparticles as carriers. *Nat. Commun.* **2013**, *4*, 1707.

(9) Lebedev, M. A.; Nicolelis, M. A. L. Brain-machine interfaces: past, present and future. *Trends Neurosci.* **2006**, *29* (9), 536−546.

(10) Hill, N. A. Why are there so few magnetic ferroelectrics? *J. Phys. Chem. B* **2000**, *104* (29), 6694−6709.

(11) Spaldin, N. A.; Pickett, W. E. Computational design of multifunctional materials. *J. Solid State Chem.* **2003**, *176* (2), 615−632.

(12) Prellier, W.; Singh, M. P.; Murugavel, P. The single-phase multiferroic oxides: from bulk to thin film (vol 17, pg 803, 2005). *J. Phys.: Condens. Matter* **2005**, *17* (48), 7753−7753.

(13) Wang, J.; Neaton, J. B.; Zheng, H.; Nagarajan, V.; Ogale, S. B.; Liu, B.; Viehland, D.; Vaithyanathan, V.; Schlom, D. G.; Waghmare, U. V.; Spaldin, N. A.; Rabe, K. M.; Wuttig, M.; Ramesh, R. Epitaxial $BiFeO_3$ multiferroic thin film heterostructures. *Science* **2003**, *299* (5613), 1719−1722.

(14) Srinivasan, G. Magnetoelectric Composites. *Annu. Rev. Mater. Res.* **2010**, *40*, 153−178.

(15) Ryu, J.; Priya, S.; Uchino, K.; Kim, H. E. Magnetoelectric effect in composites of magnetostrictive and piezoelectric materials. *J. Electroceram.* **2002**, *8* (2), 107−119.

(16) Ma, J.; Hu, J. M.; Li, Z.; Nan, C. W. Recent Progress in Multiferroic Magnetoelectric Composites: from Bulk to Thin Films. *Adv. Mater.* **2011**, *23* (9), 1062−1087.

(17) Nan, C. W.; Li, M.; Huang, J. H. Calculations of giant magnetoelectric effects in ferroic composites of rare-earth-iron alloys and ferroelectric polymers. *Phys. Rev. B* **2001**, *63* (14), 144415.

(18) Nan, C. W.; Liu, G.; Lin, Y. H. Influence of interfacial bonding on giant magnetoelectric response of multiferroic laminated composites of $Tb_{1-x}Dy_xFe_2$ and $PbZr_xTi_{1-x}O_3$. *Appl. Phys. Lett.* **2003**, *83* (21), 4366−4368.

(19) Srinivasan, G.; Rasmussen, E. T.; Gallegos, J.; Srinivasan, R.; Bokhan, Y. I.; Laletin, V. M. Magnetoelectric bilayer and multilayer structures of magnetostrictive and piezoelectric oxides. *Phys. Rev. B* **2001**, *64* (2), 214408.

(20) Ryu, J.; Carazo, A. V.; Uchino, K.; Kim, H. E. Magnetoelectric properties in piezoelectric and magnetostrictive laminate composites. *Jpn. J. Appl. Phys. 1* **2001**, *40* (8), 4948−4951.

https://dx.doi.org/10.1021/acs.nanolett.0c01588
Nano Lett. XXXX, XXX, XXX−XXX

(21) Hohenberger, S.; Lazenka, V.; Selle, S.; Patzig, C.; Temst, K.; Lorenz, M. Magnetoelectric Coupling in Epitaxial Multiferroic $BiFeO_3$-$BaTiO_3$ Composite Thin Films. *Phys. Status Solidi B* **2020**, *257*, 1900613.
(22) Lorenz, M.; Lazenka, V.; Schwinkendorf, P.; Bern, F.; Ziese, M.; Modarresi, H.; Volodin, A.; Van Bael, M. J.; Temst, K.; Vantomme, A.; Grundmann, M. Multiferroic $BaTiO_3$-$BiFeO_3$ composite thin films and multilayers: strain engineering and magnetoelectric coupling. *J. Phys. D: Appl. Phys.* **2014**, *47* (13), 135303.
(23) Lorenz, M.; Hirsch, D.; Patzig, C.; Hoche, T.; Hohenberger, S.; Hochmuth, H.; Lazenka, V.; Temst, K.; Grundmann, M. Correlation of Interface Impurities and Chemical Gradients with High Magnetoelectric Coupling Strength in Multiferroic $BiFeO_3$-$BaTiO_3$ Superlattices. *ACS Appl. Mater. Interfaces* **2017**, *9* (22), 18956−18965.
(24) Jochum, J. K.; Lorenz, M.; Gunnlaugsson, H. P.; Patzig, C.; Hoche, T.; Grundmann, M.; Vantomme, A.; Temst, K.; Van Bael, M. J.; Lazenka, V. Impact of magnetization and hyperfine field distribution on high magnetoelectric coupling strength in $BaTiO_3$-$BiFeO_3$ multilayers. *Nanoscale* **2018**, *10* (12), 5574−5580.
(25) Hohenberger, S.; Lazenka, V.; Temst, K.; Selle, S.; Patzig, C.; Hoche, T.; Grundmann, M.; Lorenz, M. Effect of double layer thickness on magnetoelectric coupling in multiferroic $BaTiO_3$-$Bi_{0.95}Gd_{0.05}FeO_3$ multilayers. *J. Phys. D: Appl. Phys.* **2018**, *51* (18), 184002.
(26) Liu, X. M.; Fu, S. Y.; Huang, C. J. Synthesis and magnetic characterization of novel $CoFe_2O_4$-$BiFeO_3$ nanocomposites. *Mater. Sci. Eng., B* **2005**, *121* (3), 255−260.
(27) Mahajan, R. P.; Patankar, K. K.; Kothale, M. B.; Patil, S. A. Conductivity, dielectric behaviour and magnetoelectric effect in copper ferrite-barium titanate composites. *Bull. Mater. Sci.* **2000**, *23* (4), 273−279.
(28) Grossinger, R.; Duong, G. V.; Sato-Turtelli, R. The physics of magnetoelectric composites. *J. Magn. Magn. Mater.* **2008**, *320* (14), 1972−1977.
(29) Zheng, H.; Wang, J.; Lofland, S. E.; Ma, Z.; Mohaddes-Ardabili, L.; Zhao, T.; Salamanca-Riba, L.; Shinde, S. R.; Ogale, S. B.; Bai, F.; Viehland, D.; Jia, Y.; Schlom, D. G.; Wuttig, M.; Roytburd, A.; Ramesh, R. Multiferroic $BaTiO_3$-$CoFe_2O_4$ nanostructures. *Science* **2004**, *303* (5658), 661−663.
(30) Kemmer, N. Collected Papers of L.D. Landau. *Proc. Phys. Soc., London* **1966**, *88*, 247.
(31) Tilley, D. R.; Zeks, B. Landau Theory of Phase-Transitions in Thick-Films. *Solid State Commun.* **1984**, *49* (8), 823−827.
(32) Ahn, C. H.; Rabe, K. M.; Triscone, J. M. Ferroelectricity at the nanoscale: Local polarization in oxide thin films and heterostructures. *Science* **2004**, *303* (5657), 488−491.
(33) Nan, C. W. The analysis of piezoelectric/piezomagnetic composite materials containing ellipsoidal inclusions - Comment. *J. Appl. Phys.* **1997**, *82* (10), 5268−5269.
(34) Huang, J. H.; Kuo, W. S. The analysis of piezoelectric/piezomagnetic composite materials containing ellipsoidal inclusions - Reply. *J. Appl. Phys.* **1997**, *82* (10), 5270−5270.
(35) Zhai, J. Y.; Cai, N.; Shi, Z.; Lin, Y. H.; Nan, C. W. Magnetic-dielectric properties of $NiFe_2O_4$/PZT particulate composites. *J. Phys. D: Appl. Phys.* **2004**, *37* (6), 823−827.
(36) Bueno-Baques, D.; Hurtado-Lopez, G.; Corral-Flores, V.; Gomez, S.; Diley, N. R.; Glushchenko, A. Development of a new module for the measurement of the magneto-electric direct and converse effects based on an alternating current susceptometer. *Rev. Sci. Instrum.* **2014**, *85* (8), 085116.
(37) Shen, X. D.; Zhou, L.; Chai, Y. S.; Wu, Y.; Liu, Z. H.; Yin, Y. Y.; Cao, H. B.; Dela Cruz, C.; Sun, Y.; Jin, C. Q.; Munoz, A.; Alonso, J. A.; Long, Y. W. Large linear magnetoelectric effect and field-induced ferromagnetism and ferroelectricity in $DyCrO_4$. *NPG Asia Mater.* **2019**, *11*, 50.
(38) Srinivasan, G.; Rasmussen, E. T.; Gallegos, J.; Srinivasan, R.; Bokhan, Y. I.; Laletin, V. M. Magnetoelectric bilayer and multilayer structures of magnetostrictive and piezoelectric oxides. *Phys. Rev. B* **2001**, *64* (21), 214408.
(39) Srinivasan, G.; Rasmussen, E. T.; Hayes, R. Magnetoelectric effects in ferrite-lead zirconate titanate layered composites: The influence of zinc substitution in ferrites. *Phys. Rev. B* **2003**, *67* (1), 014418.
(40) Ryu, J.; Carazo, A. V.; Uchino, K.; Kim, H. E. Piezoelectric and magnetoelectric properties of Lead Zirconate Titanate/Ni-Ferrite particulate composites. *J. Electroceram.* **2001**, *7* (1), 17−24.
(41) Srinivas, S.; Li, J. Y. The effective magnetoelectric coefficients of polycrystalline multiferroic composites. *Acta Mater.* **2005**, *53* (15), 4135−4142.
(42) Nan, C. W.; Bichurin, M. I.; Dong, S. X.; Viehland, D.; Srinivasan, G. Multiferroic magnetoelectric composites: Historical perspective, status, and future directions. *J. Appl. Phys.* **2008**, *103* (3), 031101.
(43) Devan, R. S.; Chougule, B. K. Effect of composition on coupled electric, magnetic, and dielectric properties of two phase particulate magnetoelectric composite. *J. Appl. Phys.* **2007**, *101* (1), 014109.
(44) Dong, S. X.; Zhai, J. Y.; Li, J. F.; Viehland, D.; Summers, E. Strong magnetoelectric charge coupling in stress-biased multilayer-piezoelectric/magnetostrictive composites. *J. Appl. Phys.* **2007**, *101* (12), 124102.
(45) Xing, Z. P.; Dong, S. X.; Zhai, J. Y.; Yan, L.; Li, J. F.; Viehland, D. Resonant bending mode of Terfenol-D/steel/$Pb(Zr,Ti)O_3$ magnetoelectric laminate composites. *Appl. Phys. Lett.* **2006**, *89* (11), 112911.
(46) Zhai, J. Y.; Dong, S. X.; Xing, Z. P.; Li, J. F.; Viehland, D. Giant magnetoelectric effect in Metglas/polyvinylidene-fluoride laminates. *Appl. Phys. Lett.* **2006**, *89* (8), 083507.
(47) Lo, C. C. H. Experimental and modeling studies of the magnetomechanical effect in substituted cobalt ferrites for magnetoelastic stress sensors. *J. Appl. Phys.* **2010**, *107* (9), 09E706.
(48) Acosta, M.; Novak, N.; Rojas, V.; Patel, S.; Vaish, R.; Koruza, J.; Rossetti, G. A.; Rodel, J. $BaTiO_3$-based piezoelectrics: Fundamentals, current status, and perspectives. *Appl. Phys. Rev.* **2017**, *4* (4), 041305.
(49) Goncalves, R.; Larrea, A.; Sebastian, M. S.; Sebastian, V.; Martins, P.; Lanceros-Mendez, S. Synthesis and size dependent magnetostrictive response of ferrite nanoparticles and their application in magnetoelectric polymer-based multiferroic sensors. *J. Mater. Chem. C* **2016**, *4* (45), 10701−10706.
(50) Wojdyr, M. Fityk: a general-purpose peak fitting program. *J. Appl. Crystallogr.* **2010**, *43*, 1126−1128.
(51) Bozorth, R. M.; Walker, J. G. Magnetostriction of Single Crystals of Cobalt and Nickel Ferrites. *Phys. Rev.* **1952**, *88* (5), 1209−1209.
(52) Smith, A. B.; Jones, R. V. Magnetostriction in Nickel Ferrite and Cobalt-Nickel Ferrite. *J. Appl. Phys.* **1966**, *37* (3), 1001.
(53) Khizroev, S.; Litvinov, D. Perpendicular magnetic recording: Writing process. *J. Appl. Phys.* **2004**, *95* (9), 4521−4537.
(54) Bichurin, M. I.; Petrov, V. M.; Srinivasan, G. Theory of low-frequency magnetoelectric effects in ferromagnetic-ferroelectric layered composites. *J. Appl. Phys.* **2002**, *92* (12), 7681−7683.
(55) Nan, C. W. Magnetoelectric Effect in Composites of Piezoelectric and Piezomagnetic Phases. *Phys. Rev. B: Condens. Matter Mater. Phys.* **1994**, *50* (9), 6082−6088.
(56) Mahajan, R. P.; Patankar, K. K.; Kothale, M. B.; Chaudhari, S. C.; Mathe, V. L.; Patil, S. A. Magnetoelectric effect in cobalt ferrite-barium titanate composites and their electrical properties. *Pramana* **2002**, *58* (5−6), 1115−1124.
(57) Duong, G. V.; Groessinger, R.; Schoenhart, M.; Bueno-Basques, D. The lock-in technique for studying magnetoelectric effect. *J. Magn. Magn. Mater.* **2007**, *316* (2), 390−393.

https://dx.doi.org/10.1021/acs.nanolett.0c01588
Nano Lett. XXXX, XXX, XXX−XXX